August 8th, 2024,

Dear EarthArXiv Editors:

On behalf of myself and my co-authors, I submit our original research article “The Origin of Forearc Depressions” for consideration for publication as a non-peer reviewed preprint in EarthArXiv. The manuscript was submitted to Geology and was rejected, and is now being edited for submission to Terra Nova. The attached manuscript reflects that of our submission to Geology.

Please address all correspondence regarding this manuscript to me at chuqiaoh@sfu.ca.

Thank you for your consideration.

Sincerely,

Mr. Chuqiao Huang (chuqiaoh@sfu.ca)
Ph.D. Candidate, Simon Fraser University

Dr. Shahin E. Dashtgard (shahin_dashtgard@sfu.ca)
Professor, Simon Fraser University

Dr. H. Daniel Gibson (hdgibson@sfu.ca)
Professor, Simon Fraser University

Dr. Andrew J. Calvert (acalvert@sfu.ca)
Professor, Simon Fraser University

The origin of forearc depressions

Chuqiao Huang[1], Shahin E. Dashtgard[1], H. Daniel Gibson[1], Andrew J. Calvert[1]

[1]Department of Earth Sciences, Simon Fraser University, 8888 University Dr., Burnaby, British Columbia, Canada, V5A 1S6

Correspondence: Chuqiao Huang (Chuqiaoh@sfu.ca)

ABSTRACT

Forearc depressions form over continental subduction zones with young, slowly subducting slabs and thick trench fills. They are bound seaward by a coast range and landward by a volcanic arc such that subsidence in forearc depressions occurs between orogens and in areas characterized by plate convergence. We propose a model for forearc depression formation based on geophysical and seismic data from four circum-Pacific subduction zones. Coast range crests coincide with >100 mGal gravity anomalies, which are attributed to underplated material and indicate that underplating drives coast range uplift. Coast range crests are situated near the down-dip termini of megathrust earthquake rupture zones, showing that coast ranges overlie where subduction interface sliding behaviour transitions from frictional to semi-frictional. This transition causes subduction interface shear stress to begin decreasing with depth and triggers underplating as shear stress becomes insufficient to drag buoyant material deeper. Forearc depressions are situated landward of inter-plate seismic phenomena, indicating they overlie the hydrated forearc mantle. Forearc depressions form as counter-flexural basins over the hydrated forearc mantle; in this position the upper plate crust is not supported by the flexurally rigid slab and can bend downwards. Forearc depressions do not form over old slabs because old slabs do not exceed the temperature threshold for semi-frictional sliding prior to intersecting the mantle wedge corner. Fast convergence rates and thin trench fills promote subduction erosion along the subduction interface, thereby prohibiting the formation of coast ranges, and by extension, forearc depressions.

INTRODUCTION

Forearc depressions (Fig. 1) are a type of forearc basin and form over continental subduction zones with young (typically <30 Ma), slowly subducting (<65 mm yr^{-1}) slabs and thick trench sediment fills (>2.5 km). Forearc depressions entirely overlie the upper plate and are bound seaward by a coast range and landward by a volcanic arc. Modern examples include the Seto Inland Sea of the Nankai subduction zone in Japan; the Kenai Lowlands–Cook Inlet–Sheliklof Strait of the Alaskan subduction zone in USA; the Salish–Puget–Willamette Lowland of the Cascadia subduction zone in Canada and USA; and the Central Depression of the south-central Chilean subduction zone (Fig. 2).

Forearc depressions are narrow (typically 75 km trench-orthogonal width) with km-scale thick basin fills and are sandwiched between areas of km-scale uplift. Their formation is challenging to explain as proposed hypotheses must address how forearc depressions form between orogens and in regions characterized by plate convergence. Recently, Menant et al. (2019, 2020) used computer modelling to hypothesize that fluid escape from the subduction channel increases subduction interface shear stress, which triggers underplating. Underplating drives coast range uplift, which then causes downwards counter-flexure of the upper plate crust and forearc depression formation. Here, we revise the model of Menant et al. (2019, 2020) using empirical data to show that changes in subduction interface rheology decreases shear stress and triggers underplating, and that a young, slowly subducting slab and thick trench cover are required for this process. We also show that forearc depressions are situated over the hydrated forearc mantle and cannot form seaward of the mantle wedge corner. For clarity, we use ‘coast range’ to refer to forearc highs that form through underplating and not through other mechanisms, such as over-thrusting of the accretionary prism (e.g., the Sunda Subduction Zone; Mukti et al., 2021).

Subduction interface shear stress varies with depth and as a function of sliding behaviour. In warm subduction zones, which includes those with young slabs, the subduction interface can be divided into

frictional, semi-frictional, and stable sliding domains (Fig. 1) and the locations of these domains can be inferred by their differing seismic behaviours. Shear stress peaks and begins to decrease in the transition between the frictional and semi-frictional domains (Gao and Wang, 2017).

In the frictional domain (Fig. 1), shear stress increases with depth (Gao and Wang, 2017) because frictional strength increases with normal stress. The frictional domain defines the seismogenic zone wherein megathrust earthquakes nucleate and propagate. The up-dip limit (seaward and shallower) of the frictional domain depends on subduction interface temperature and mineralogy and can extend to the seafloor (Roesner et al., 2020; Stanislowski et al., 2022). The down-dip limit (landward and deeper) of the frictional domain corresponds to where the subduction interface exceeds 300–400 ºC whereupon quartz and feldspar begin to exhibit crystalline plasticity (Hyndman et al., 1997; Oleskevich et al., 1999).

In the semi-frictional domain (Fig. 1), shear stress decreases with depth (Gao and Wang, 2017) because ductile strength decreases with temperature. Megathrust earthquakes cannot propagate into the semi-frictional domain due to its rate-strengthening nature, and viscous processes cause slow-slip events (Schwartz and Rokosky, 2007). Very young slabs (<20 Ma) additionally experience metamorphic dehydration reactions at shallow depths (<50 km; Condit et al., 2020); this releases slab fluids that are trapped beneath an impermeable subduction interface. Trapped fluids greatly lower shear stress (Gao and Wang, 2017) and lowered shear stress generates episodic tremor and slip that clusters around the mantle wedge corner (Shelly et al., 2006; Calvert et al., 2020).

In the stable-sliding domain (Fig. 1), shear stress is low and the subduction interface is aseismic. The up-dip limit of the stable-sliding domain is where the slab contacts the hydrated forearc mantle and free water is limited. Antigorite, the high pressure form of serpentinite (Schwartz et al., 2013), deforms by vicious processes at inter-seismic strain rates (Tulley et al., 2022) and cannot accumulate the stress required to initiate megathrust earthquakes.

Subduction interface shear stress is determined using the seismic behaviour of different sliding domains, and hence, we examine geophysical and seismic data from subduction zones that host forearc depressions. For each system, we compile data on topography and bathymetry, convergence rates, slab ages, free-air gravitational anomalies, megathrust earthquake epicenter and rupture zones, tremor epicenters, and top-of-slab depth (Supplementary Data File 1). We map and interpret these data to establish how underplating, subduction interface shear stress distribution, and the location of the mantle wedge corner drive coast range and forearc depression formation. We also show why young, slowly subducting slabs and thick trench cover are required for coast range and forearc depression formation.

CHARACTERIZATION OF FOREARC DEPRESSIONS

In the Menant et al. (2019, 2020) model, underplating uplifts the overlying crust and generates a coast range. Gravity anomalies increase towards the coast range crest to >100 mGal, and increasing gravity anomalies are attributed to underplated material (Bassett and Watts, 2015) (Figs. 3A–D). Specifically, underplating causes uncompensated crustal thickening, which increases free-air gravity anomalies. Increasing gravity anomalies associated with coast ranges coincide with km-scale reflector bands that are interpreted as underplated material (Calvert et al., 2006; Kimura et al., 2010; Scholl, 2021; Delph et al., 2021).

Coast ranges also overlie where subduction interface shear stress begins to decrease with depth, which is evident in the position of coast range topographic crests near the down-dip termini of megathrust earthquake rupture zones (Figs. 3E–H). In warm subduction zones, megathrust earthquakes only propagate in the frictional domain of the subduction interface (Fig. 1) and rupture zones terminate in the transition between the frictional and semi-frictional domains. This transition is also where shear stress changes from increasing with depth to decreasing with depth. There is no direct evidence from Cascadia that shows the coast range overlying the down-dip termini of megathrust earthquake rupture zones

because the last megathrust earthquake occurred prior to modern record keeping (in 1700). However, geodetically inferred interseismic locking models for Cascadia predict that subduction interface locking (i.e., the predicted megathrust earthquake rupture zone) decreases to <10% beneath Cascadia's coast range (Li et al., 2018; Lindsey et al., 2021), which is consistent with a transition from frictional to semi-frictional sliding along the subduction interface.

The location of coast range topographic crests over where shear stress begins decreasing with depth indicates that decreasing shear stress triggers the underplating necessary for coast range uplift. Underplating occurs because shear stress becomes insufficient to drag buoyant material within the subduction interface deeper.

All forearc depressions are situated landward of inter-plate seismic activity, showing they are situated landward of the mantle wedge corner (Figs. 3E–H). In warm subduction zones, megathrust earthquakes only propagate within the frictional sliding domain, which only exists where the slab is beneath the upper plate crust and not the mantle (Fig. 1). As well, Nankai (Shelly et al., 2006) and Cascadia (Calvert et al., 2020) experience episodic tremor and slip (Figs. 3E and G), and tremor epicenters cluster around the mantle wedge corner (Fig. 1). The distribution of both megathrust earthquake rupture zones and tremors seaward of forearc depressions show that all forearc depressions are situated landward of the mantle wedge corner.

Underplating causes the overlying crust to flex upwards (Menant et al., 2020) and this upwards flexure must be compensated by downwards flexure elsewhere. This cannot occur seaward of the mantle wedge corner as the upper plate crust is supported through direct contact with the flexurally rigid slab. Landward of the mantle wedge corner, the upper plate crust is no longer supported by physical contact with the slab and so it can flex downwards to form the forearc depression.

The transition from frictional to semi-frictional sliding and the associated decrease in shear stress that triggers underplating requires a young slab (<30 Ma; Fig. 2). Old slabs do not reach the temperature threshold for transition between frictional and semi-frictional sliding prior to intersecting the mantle wedge corner. As well, old slabs do not experience substantial metamorphic dehydration until they are beneath the arc (Condit et al., 2020), which leads to a dry, antigorite-poor forearc mantle (Abers et al., 2017; Wang et al., 2022). Consequently, old slabs are characterized by a single frictional domain wherein shear stress increases with depth well into the forearc mantle. Old slabs also exhibit different seismic behaviours: without a semi-frictional domain to resist the propagation of megathrust earthquakes (Schwartz and Rokosky, 2007), rupture zones can extend into the hydrated forearc mantle (Brantut et al., 2016). The exception to the relationship between slab age and subduction interface rheology described above is Alaska, where the Pacific Plate is 35–50 Ma at the trench (Fig. 2B). The Pacific slab undergoes flat subduction for 200–300 km over which it heats and exceeds 400 °C prior to intersecting the mantle wedge corner (Qu et al., 2022).

A thick trench cover (>2.5 km) is required for coast range uplift through underplating because trench sediments ultimately become the primary underplated material. For example, in the Central American Subduction Zone, the subducting Cocos Plate is 0–25 Ma at the trench. The subduction zone experiences SSEs and ETS (Baba et al., 2021), which shows the existence of a semi-frictional domain. However, neither a coast range nor forearc depression are developed, and instead, a single, broad forearc basin stretches from the shoreline to the trench. This is attributed to thin trench sediment cover (<0.5 km; Clift and Vannucchi, 2004), which provides insufficient material to underplate and generate a coast range. In contrast, subduction zones that host forearc depressions possess thick trench sediment covers (2.5–3.5 km; Clift and Vannucchi, 2004) which provide sufficient material for underplating.

Finally, a slow subduction rate (<65 mm yr^{-1}; Fig. 2) is required for forearc depression formation. At faster convergence rates, tectonic erosion dominates along the subduction interface (Clift and Vannucchi, 2004) and underplating is suppressed; this inhibits the formation of a coast range.

FORMATION OF FOREARC DEPRESSIONS

Subduction zones with forearc depressions include an additional forearc basin over the accretionary prism (Fig. 4). However, barring Nankai, for which subduction initiated recently (15 Ma; Moreno et al., 2023), all subduction zones investigated here formerly comprised a single forearc basin that stretched from the coastline to the trench. This is indicated by older strata within forearc depressions that correlate to coeval strata over and/or seaward of the coast range (England and Bustin, 1998; Encinas et al., 2012; LePain et al., 2014; Scanlon et al., 2021; Darin et al., 2022). For example, the Georgia Basin is the northern-most forearc depression of Cascadia, and its basal succession is the Nanaimo Group, a >3 km thick succession of primarily Upper Cretaceous strata (England and Bustin, 1998; Girotto et al., 2024). The Nanaimo Group is covered by >3 km of Cenozoic strata in the Georgia Basin; however, Nanaimo Group strata, including trench orthogonal-oriented deep-marine turbidites, are exposed on Vancouver Island, which is the associated coast range. This distribution of strata indicates that for much of Nanaimo Group deposition, no trench-parallel topographic barrier existed, and sedimentation occurred in a single, broad forearc basin. Based on this, we propose the following model for the formation of forearc depressions (Fig. 4):

1) Prior to forearc depression formation, a single forearc basin stretches from the shoreline to the trench and is dominated by deep-marine depositional systems and trench-orthogonal drainage (e.g., south Cascadia in the Eocene; Santra et al., 2013). Coast range uplift is suppressed by unsuitable subduction parameters such as an old slab, thin trench sediment cover, and/or high convergence rate (Fig. 4A).

2) Increases in trench sedimentation, decreases in slab age, and/or decreases in convergence rate initiate underplating. The accretionary prism grows, leading the frictional domain to shift seaward as a thick blanket of sediment insulates the slab. Underplating focuses over the transition between the frictional and semi-frictional domains, which uplifts the overlying crust to generate a coast range. The coast range divides the overlying forearc basin in two (Fig. 4B).
3) Repeated underplating leads to further coast range uplift. Forearc strata overlying the coast range are uplifted, eroded, and re-incorporated into the flanking forearc basins (e.g., south Cascadia in the Oligocene; Darin et al., 2022). Flexural counter bending occurs over the hydrated forearc mantle generating a forearc depression (Menant et al., 2020). Sedimentation in the forearc depression is dominated by continental- and shallow-marine depositional systems and trench-parallel drainage (Fig. 4C).

ACKNOWLEDGEMENTS

The authors thank the reviewers, ___, ___, and the editor ___, whose comments improved the quality of this manuscript. The authors thank Kelin Wang of the Geological Society of Canada whose ideas greatly improved this manuscript, and Evangeline Lapalme for her guidance with ArcGIS Pro. This study was funded through a Natural Sciences and Engineering Research Council of Canada Discovery Grant to Dr. Shahin Dashtgard (RGPIN-2019-04528).

REFERENCES CITED

Abers, G.A., van Keken, P.E., and Hacker, B.R., 2017, The cold and relatively dry nature of mantle forearcs in subduction zones: Nature Geoscience, v. 10, p. 333–337, doi:10.1038/ngeo2922.

Baba, S., Obara, K., Takemura, S., Takeo, A., and Abers, G.A., 2021, Shallow Slow Earthquake Episodes Near the Trench Axis off Costa Rica: Journal of Geophysical Research: Solid Earth, v. 126, p. e2021JB021706, doi:10.1029/2021JB021706.

Bassett, D., and Watts, A.B., 2015, Gravity anomalies, crustal structure, and seismicity at subduction zones: 2. Interrelationships between fore-arc structure and seismogenic behavior: CRUSTAL STRUCTURE AND SEISMICITY: 2. FORE-ARC STRUCTURE: Geochemistry, Geophysics, Geosystems, v. 16, p. 1541–1576, doi:10.1002/2014GC005685.

Brantut, N., Passelègue, F.X., Deldicque, D., Rouzaud, J.-N., and Schubnel, A., 2016, Dynamic weakening and amorphization in serpentinite during laboratory earthquakes: Geology, v. 44, p. 607–610, doi:10.1130/G37932.1.

Calvert, A.J., Bostock, M.G., Savard, G., and Unsworth, M.J., 2020, Cascadia low frequency earthquakes at the base of an overpressured subduction shear zone: Nature Communications, v. 11, p. 3874, doi:10.1038/s41467-020-17609-3.

Calvert, A.J., Ramachandran, K., Kao, H., and Fisher, M.A., 2006, Local thickening of the Cascadia forearc crust and the origin of seismic reflectors in the uppermost mantle: Seismic Probing of Continents and their Margins, v. 420, p. 175–188, doi:10.1016/j.tecto.2006.01.021.

Clift, P., and Vannucchi, P., 2004, Controls on tectonic accretion versus erosion in subduction zones: Implications for the origin and recycling of the continental crust: Reviews of Geophysics, v. 42, doi:10.1029/2003RG000127.

Condit, C.B., Guevara, V.E., Delph, J.R., and French, M.E., 2020, Slab dehydration in warm subduction zones at depths of episodic slip and tremor: Earth and Planetary Science Letters, v. 552, p. 116601, doi:10.1016/j.epsl.2020.116601.

Darin, M.H., Armentrout, J.M., and Dorsey, R.J., 2022, Oligocene onset of uplift and inversion of the Cascadia forearc basin, southern Oregon Coast Range, USA: Geology, v. 50, p. 603–609, doi:10.1130/G49925.1.

Delph, J.R., Thomas, A.M., and Levander, A., 2021, Subcretionary tectonics: Linking variability in the expression of subduction along the Cascadia forearc: Earth and Planetary Science Letters, v. 556, p. 116724, doi:10.1016/j.epsl.2020.116724.

Encinas, A., Finger, K.L., Buatois, L.A., and Peterson, D.E., 2012, Major forearc subsidence and deep-marine Miocene sedimentation in the present Coastal Cordillera and Longitudinal Depression of south-central Chile (38°30′S–41°45′S): GSA Bulletin, v. 124, p. 1262–1277, doi:10.1130/B30567.1.

England, T.D.J., and Bustin, R.M., 1998, Architecture of the Georgia Basin southwestern British Columbia: Bulletin of Canadian Petroleum Geology, v. 46, p. 288–320, doi:10.35767/gscpgbull.46.2.288.

Gao, X., and Wang, K., 2017, Rheological separation of the megathrust seismogenic zone and episodic tremor and slip: Nature, v. 543, p. 416–419, doi:10.1038/nature21389.

Girotto, K., Dashtgard, S.E., Huang, C., MacEachern, J.A., Gibson, H.D., and Cathyl-Huhn, G., 2024, Stratigraphy, palaeogeography and evolution of the lower Nanaimo Group (Cretaceous), Georgia Basin, Canada: Basin Research, v. 36, p. e12830, doi:10.1111/bre.12830.

Hyndman, R.D., Yamano, M., and Oleskevich, D.A., 1997, The seismogenic zone of subduction thrust faults: The Island Arc, v. 6, p. 244–260, doi:10.1111/j.1440-1738.1997.tb00175.x.

Kimura, H., Takeda, T., Obara, K., and Kasahara, K., 2010, Seismic Evidence for Active Underplating Below the Megathrust Earthquake Zone in Japan: Science, v. 329, p. 210–212, doi:10.1126/science.1187115.

LePain, D.L., Stanley, R.G., Helmold, K.P., and Shellenbaum, D.P., 2014, Geologic Framework and Petroleum Systems of Cook Inlet Basin, South-Central Alaska, *in* Stone, D.M. and Hite, D.M.

eds., Oil and Gas Fields of the Cook Inlet Basin, Alaska, American Association of Petroleum Geologists, v. 104, p. 0, doi:10.1306/13491874M1043621.

Li, S., Wang, K., Wang, Y., Jiang, Y., and Dosso, S.E., 2018, Geodetically Inferred Locking State of the Cascadia Megathrust Based on a Viscoelastic Earth Model: Journal of Geophysical Research: Solid Earth, v. 123, p. 8056–8072, doi:10.1029/2018JB015620.

Lindsey, E.O., Mallick, R., Hubbard, J.A., Bradley, K.E., Almeida, R.V., Moore, J.D.P., Bürgmann, R., and Hill, E.M., 2021, Slip rate deficit and earthquake potential on shallow megathrusts: Nature Geoscience, v. 14, p. 321–326, doi:10.1038/s41561-021-00736-x.

Menant, A., Angiboust, S., and Gerya, T., 2019, Stress-driven fluid flow controls long-term megathrust strength and deep accretionary dynamics: Scientific Reports, v. 9, p. 9714, doi:10.1038/s41598-019-46191-y.

Menant, A., Angiboust, S., Gerya, T., Lacassin, R., Simoes, M., and Grandin, R., 2020, Transient stripping of subducting slabs controls periodic forearc uplift: Nature Communications, v. 11, p. 1823, doi:10.1038/s41467-020-15580-7.

Moreno, E.J., Manea, V.C., Manea, M., Yoshioka, S., Suenaga, N., and Bayona, A., 2023, Numerical modeling of subduction and evaluation of Philippine Sea Plate tectonic history along the Nankai Trough: Scientific Reports, v. 13, p. 18313, doi:10.1038/s41598-023-45370-2.

Mukti, M.M., Maulin, H.B., and Permana, H., 2021, Growth of forearc highs and basins in the oblique Sumatra subduction system: Petroleum Exploration and Development, v. 48, p. 683–692, doi:10.1016/S1876-3804(21)60054-X.

Oleskevich, D.A., Hyndman, R.D., and Wang, K., 1999, The updip and downdip limits to great subduction earthquakes: Thermal and structural models of Cascadia, south Alaska, SW Japan, and

Chile: Journal of Geophysical Research: Solid Earth, v. 104, p. 14965–14991, doi:10.1029/1999JB900060.

Qu, R., Ji, Y., Zhu, W., Zhao, Y., and Zhu, Y., 2022, Fast and Slow Earthquakes in Alaska: Implications from a Three-Dimensional Thermal Regime and Slab Metamorphism: Applied Sciences, v. 12, p. 11139, doi:10.3390/app122111139.

Roesner, A., Ikari, M.J., Saffer, D.M., Stanislowski, K., Eijsink, A.M., and Kopf, A.J., 2020, Friction experiments under in-situ stress reveal unexpected velocity-weakening in Nankai accretionary prism samples: Earth and Planetary Science Letters, v. 538, p. 116180, doi:10.1016/j.epsl.2020.116180.

Santra, M., Steel, R.J., Olariu, C., and Sweet, M.L., 2013, Stages of sedimentary prism development on a convergent margin — Eocene Tyee Forearc Basin, Coast Range, Oregon, USA: From Source to Sink - Quantifying the mass transfer from mountain ranges to sedimentary basins, v. 103, p. 207–231, doi:10.1016/j.gloplacha.2012.11.006.

Scanlon, D.P., Bershaw, J., Wells, R.E., and Streig, A.R., 2021, The spatial and temporal evolution of the Portland and Tualatin forearc basins, Oregon, USA: Geosphere, v. 17, p. 804–823, doi:10.1130/GES02298.1.

Scholl, D.W., 2021, Seismic imaging evidence that forearc underplating built the accretionary rock record of coastal North and South America: Geological Magazine, v. 158, p. 104–117, doi:10.1017/S0016756819000955.

Schwartz, S., Guillot, S., Reynard, B., Lafay, R., Debret, B., Nicollet, C., Lanari, P., and Auzende, A.L., 2013, Pressure–temperature estimates of the lizardite/antigorite transition in high pressure serpentinites: Lithos, v. 178, p. 197–210, doi:10.1016/j.lithos.2012.11.023.

Schwartz, S.Y., and Rokosky, J.M., 2007, Slow slip events and seismic tremor at circum-Pacific subduction zones: SLOW SLIP AND SEISMIC TREMOR: Reviews of Geophysics, v. 45, p. n/a-n/a, doi:10.1029/2006RG000208.

Shelly, D.R., Beroza, G.C., Ide, S., and Nakamula, S., 2006, Low-frequency earthquakes in Shikoku, Japan, and their relationship to episodic tremor and slip: Nature, v. 442, p. 188–191, doi:10.1038/nature04931.

Stanislowski, K., Roesner, A., and Ikari, M.J., 2022, Implications for megathrust slip behavior and pore pressure at the shallow northern Cascadia subduction zone from laboratory friction experiments: Earth and Planetary Science Letters, v. 578, p. 117297, doi:10.1016/j.epsl.2021.117297.

Tulley, C.J., Fagereng, Å., Ujiie, K., Piazolo, S., Tarling, M.S., and Mori, Y., 2022, Rheology of Naturally Deformed Antigorite Serpentinite: Strain and Strain-Rate Dependence at Mantle-Wedge Conditions: Geophysical Research Letters, v. 49, p. e2022GL098945, doi:10.1029/2022GL098945.

Wang, D., Wang, L., Zhang, R., Cai, N., Zhang, J., Chen, P., and Cao, Y., 2022, Mantle Wedge Water Contents Estimated From Ultrasonic Laboratory Measurements of Olivine-Antigorite Aggregates: Geophysical Research Letters, v. 49, p. e2022GL098226, doi:10.1029/2022GL098226.

FIGURES AND CAPTIONS

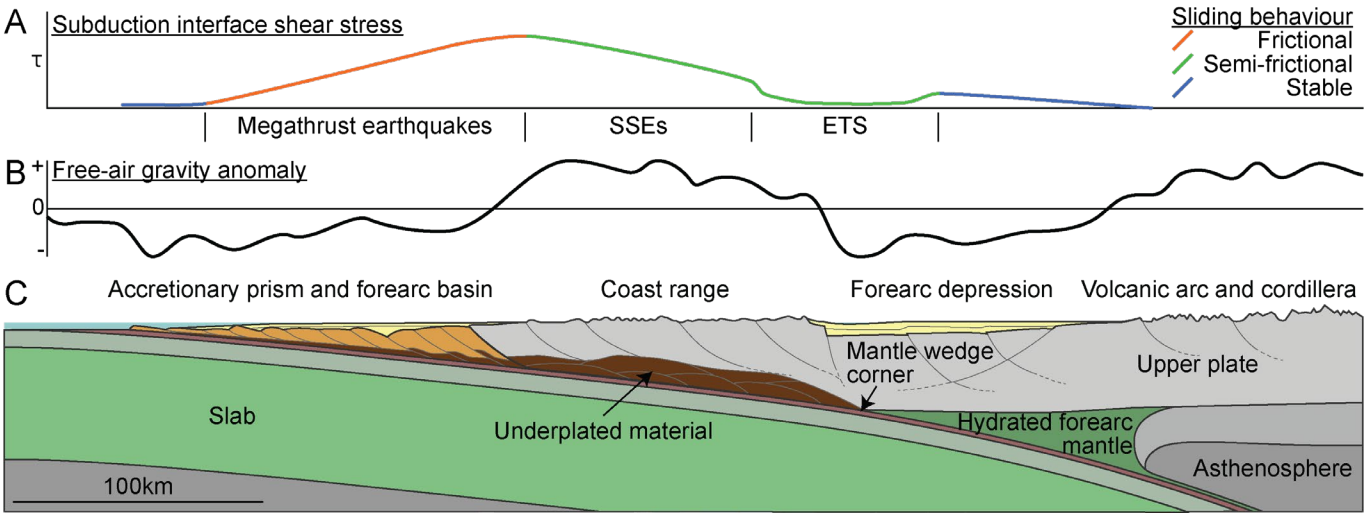

Figure 1. Schematic cross-section of a warm subduction zone hosting a forearc depression. **A)** Shear stress (τ) distribution along the subduction interface and predicted inter-plate sliding behaviour. Expected locations of inter-plate seismic events are labelled on the x-axis. Abbreviations: SSEs – slow slip events; ETS – episodic tremor and slip. **B)** Predicted free-air gravity anomaly field of the subduction zone. **C)** Major tectonic elements of the subduction zone. No vertical exaggeration.

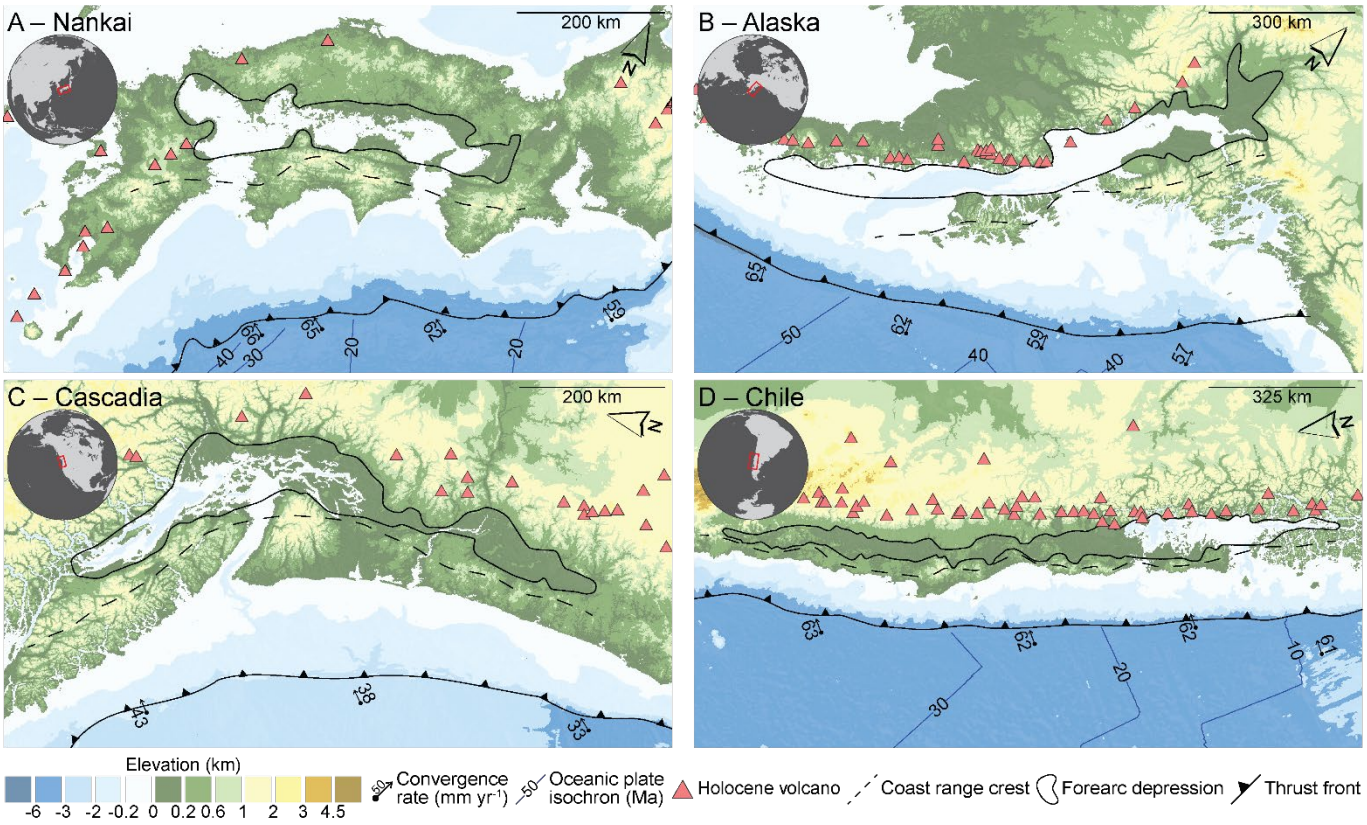

318

319 **Figure 2.** General subduction parameters of subduction zones with forearc depressions. Data shown
320 include topography/bathymetry, convergence rate with respect to a stable upper plate, oceanic plate
321 isochrons, Holocene volcanoes, coast range topographic crest, forearc depression boundary, and
322 subduction thrust front. No oceanic plate isochrons are present for Cascadia because the Juan de Fuca
323 oceanic plate is younger than 10 Ma everywhere.

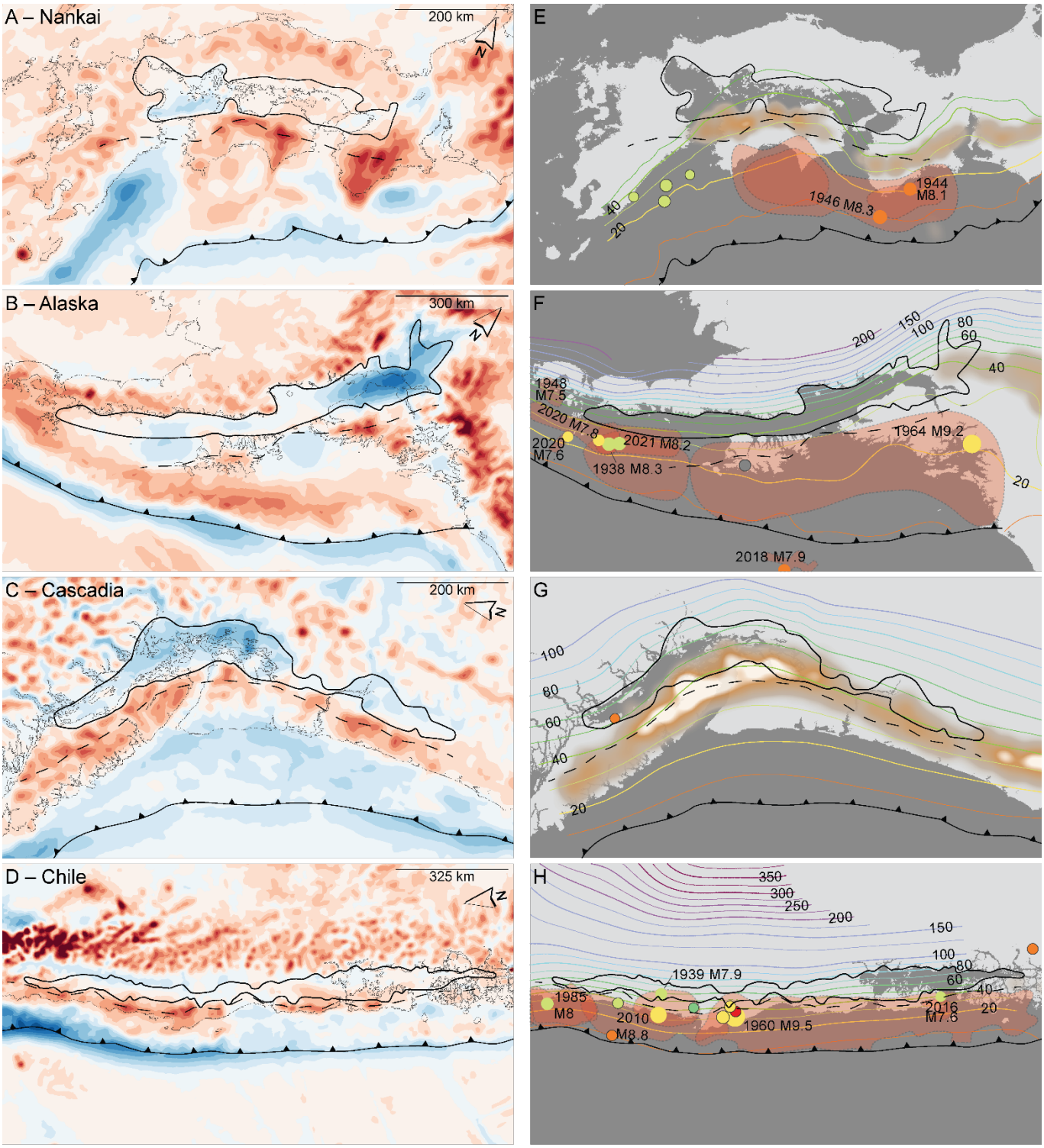
A – Nankai
200 km
B – Alaska
300 km
C – Cascadia
200 km
D – Chile
325 km
E
1944 M8.1
1946 M8.3
40
20
F
200
150
100
80
60
40
20
1948 M7.5
2020 M7.8
2021 M8.2
2020 M7.6
1938 M8.3
1964 M9.2
2018 M7.9
G
100
80
60
40
20
H
350
300
250
200
150
100
80
60
40
20
1939 M7.9
1985 M8
2010 M8.8
1960 M9.5
2016 M7.6
Free air anomaly (mGal)
-200 100 0 100 200
Earthquake epicenter and magnitude
Megathrust earthquake rupture zone
Tremor Density
Low High
Slab depth (km)
Coast range crest
Forearc depression
Thrust front

Figure 3. Geophysical and seismic data from subduction zones with forearc depressions. All maps include coast range topographic crest, forearc depression boundary, and subduction thrust front. **A–D)** Free-air gravity anomalies, scaled to ±200 mGal. **E – H)** Seismic activity. Data show include megathrust earthquake magnitudes, epicenters, and rupture zones, tremor densities, and top-of-slab depth. Megathrust earthquake epicenters and top-of-slab depth share the same colour scheme, which indicates depth. For megathrust earthquake epicenters, no circle outline means its rupture zone is depicted and an outline means it is not.

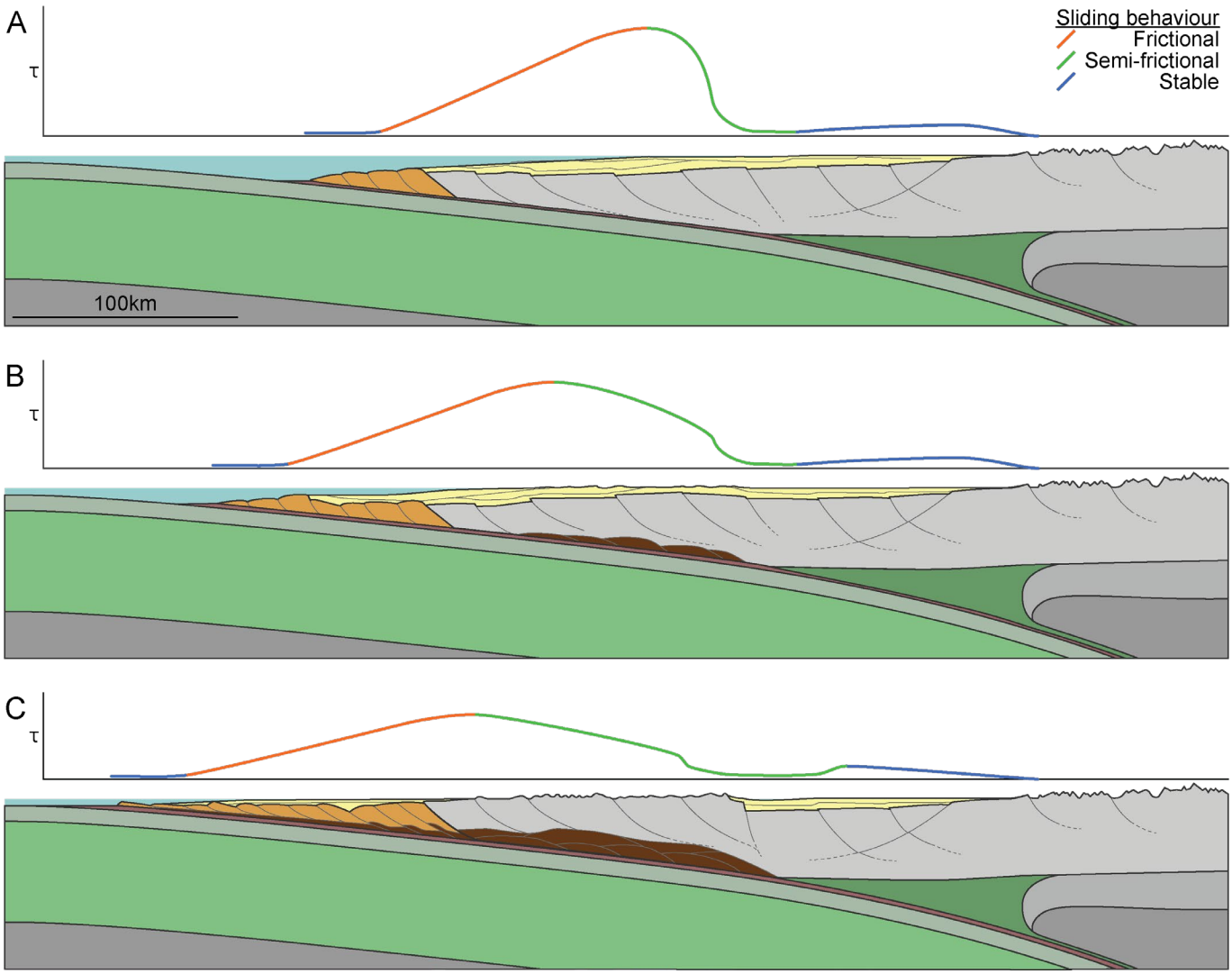

Figure 4. Schematic for the formation of a forearc depression. Time steps A–C are described in the text. Each schematic depicts the shear stress (τ) distribution along the subduction interface and predicted inter-plate sliding behaviour, and tectonic elements of the subduction zone. Legend and scale are same as figure 1. No vertical exaggeration.

SUPPLEMENTARY FILE 1: DATA SOURCES

Our study compiles and interprets publicly available data. We focus on four subduction zones globally that host forearc depressions: Nankai, Alaska, Cascadia, and Chile. For each subduction zone, we assemble and interpret three datasets: 1) general subduction parameters, 2) gravity, and 3) seismic.

GENERAL SUBDUCTION PARAMETERS

The general subduction parameters dataset comprises topographic and bathymetric data, forearc depression boundaries, Holocene volcanic centers, oceanic plate isochrons, and plate convergence rates. Topographic and bathymetric data are derived from the General Bathymetric Chart of the Oceans project (Mayer et al., 2018). Coast ranges are defined by tracing a line through the topographic crest of each coast range, and forearc depression boundaries are defined by tracing the 200m topographic contour. Holocene volcanic data is derived from the Volcanoes of the World Database (Venzke, 2023), and oceanic plate isochrons are derived from Seton et al., 2020. Plate convergence vectors are based on plate motions calculated by the Global Strain Rate Model v2.1 (Kreemer et al., 2014) and are defined with respect to a stable upper plate: for Nankai, the Philippine Sea Plate subducts beneath the stable Amur Plate; for Alaska, the Pacific Plate subducts beneath the stable North American Plate; for Cascadia, the Juan de Fuca Plate subducts beneath the stable North American Plate; and for Chile, the Nazca Plate subducts beneath the stable South American Plate.

GRAVITY DATA

Gravity data is derived from the satellite free-air gravity model of Sandwell et al. (2014). Sandwell et al. (2014) provide data in a 1 arc-minute by 1 arc-minute grid. We use kriging to generate our free-air gravity anomaly map. We normalize all gravity data to ±200 mGal because these values cover the full range of gravity anomalies from the trench to the volcanic arcs of the subduction zones investigated

herein. While some areas, such as the Bonin trench and volcanic arc (Fig. 3A), have anomalies more than ±300 mGal, these higher values are not portrayed because they are not relevant to this study.

SEISMIC DATA

Seismic data includes megathrust earthquake epicenters and rupture zones, tremor epicenters, and top-of-slab depth data. Megathrust earthquake epicenters are derived from the USGS earthquake catalog for all earthquakes that: 1) occurred between 1900 and 2023, 2) exceeded 7.5 magnitude; and, 3) were shallower than 70 km. These search parameters filter out most other earthquake types that occur near subduction zones, such as intra-slab and intra-crust earthquakes. Megathrust rupture zone data are compiled from a variety of sources. For Nankai, rupture zones are calculated by Ando (1975). For Alaska, rupture zones are derived from the Alaska Earthquake Center. For Chile, rupture zones are compiled from Kelleher (1972), Sparkes et al. (2010), and Hicks et al. (2014).

Tremor data is compiled from multiple sources. For Nankai, tremor data is from the World Tremor Database generated by Idehara et al. (2014). For Alaska, tremors are from Wech (2016). For Cascadia, tremors are derived from the Pacific Northwest Seismic Network's tremor catalog (Wech, 2021) for all events occurring between August 6, 2009 and September 4, 2023. For Chile, tremor data are derived from the World Tremor Database, which combines data from Idehara et al. (2014), Yabe and Ide (2014), and Pastén-Araya et al. (2022) . Slab depth data are from Nakanishi et al. (2018) for Nankai, McCrory et al. (2012) for Cascadia, and the Slab 2.0 model of Hayes et al. (2018) for Alaska and Chile.

BIBLIOGRAPHY

Alaska Earthquake Center, 2023, Earthquake Map:, https://earthquake.alaska.edu/earthquakes.

Ando, M., 1975, Source mechanisms and tectonic significance of historical earthquakes along the nankai trough, Japan: Tectonophysics, v. 27, p. 119–140, doi:10.1016/0040-1951(75)90102-X.

Hayes, G.P., Moore, G.L., Portner, D.E., Hearne, M., Flamme, H., Furtney, M., and Smoczyk, G.M., 2018, Slab2, a comprehensive subduction zone geometry model: Science, v. 362, p. 58–61, doi:10.1126/science.aat4723.

Hicks, S.P., Rietbrock, A., Ryder, I.M.A., Lee, C.-S., and Miller, M., 2014, Anatomy of a megathrust: The 2010 M8.8 Maule, Chile earthquake rupture zone imaged using seismic tomography: Earth and Planetary Science Letters, v. 405, p. 142–155, doi:10.1016/j.epsl.2014.08.028.

Idehara, K., Yabe, S., and Ide, S., 2014, Regional and global variations in the temporal clustering of tectonic tremor activity: Earth, Planets and Space, v. 66, p. 66, doi:10.1186/1880-5981-66-66.

Kelleher, J.A., 1972, Rupture zones of large South American earthquakes and some predictions: Journal of Geophysical Research (1896-1977), v. 77, p. 2087–2103, doi:10.1029/JB077i011p02087.

Kreemer, C., Blewitt, G., and Klein, E.C., 2014, A geodetic plate motion and Global Strain Rate Model: Geochemistry, Geophysics, Geosystems, v. 15, p. 3849–3889, doi:10.1002/2014GC005407.

Mayer, L., Jakobsson, M., Allen, G., Dorschel, B., Falconer, R., Ferrini, V., Lamarche, G., Snaith, H., and Weatherall, P., 2018, The Nippon Foundation—GEBCO Seabed 2030 Project: The Quest to See the World's Oceans Completely Mapped by 2030: Geosciences, v. 8, doi:10.3390/geosciences8020063.

McCrory, P.A., Blair, J.L., Waldhauser, F., and Oppenheimer, D.H., 2012, Juan de Fuca slab geometry and its relation to Wadati-Benioff zone seismicity: Journal of Geophysical Research: Solid Earth, v. 117, doi:10.1029/2012JB009407.

Nakanishi, A., Takahashi, N., Yamamoto, Y., Takahashi, T., Ozgur Citak, S., Nakamura, T., Obana, K., Kodaira, S., and Kaneda, Y., 2018, Three-dimensional plate geometry and P-wave velocity models of the subduction zone in SW Japan: Implications for seismogenesis, *in* Byrne, T., Underwood, M.B., III, Fisher, D., McNeill, L., Saffer, D., Ujiie, K., and Yamaguchi, A. eds., Geology and Tectonics of Subduction Zones: A Tribute to Gaku Kimura, Geological Society of America, v. 534, p. 0, doi:10.1130/2018.2534(04).

Pastén-Araya, F. et al., 2022, Along-Dip Segmentation of the Slip Behavior and Rheology of the Copiapó Ridge Subducted in North-Central Chile: Geophysical Research Letters, v. 49, p. e2021GL095471, doi:10.1029/2021GL095471.

Sandwell, D.T., Müller, R.D., Smith, W.H.F., Garcia, E., and Francis, R., 2014, New global marine gravity model from CryoSat-2 and Jason-1 reveals buried tectonic structure: Science, v. 346, p. 65–67, doi:10.1126/science.1258213.

Seton, M., Müller, R.D., Zahirovic, S., Williams, S., Wright, N.M., Cannon, J., Whittaker, J.M., Matthews, K.J., and McGirr, R., 2020, A Global Data Set of Present-Day Oceanic Crustal Age and Seafloor Spreading Parameters: Geochemistry, Geophysics, Geosystems, v. 21, p. e2020GC009214, doi:10.1029/2020GC009214.

Sparkes, R., Tilmann, F., Hovius, N., and Hillier, J., 2010, Subducted seafloor relief stops rupture in South American great earthquakes: Implications for rupture behaviour in the 2010 Maule, Chile earthquake: Earth and Planetary Science Letters, v. 298, p. 89–94, doi:10.1016/j.epsl.2010.07.029.

United States Geological Survey USGS Earthquake Catalog:, https://earthquake.usgs.gov/earthquakes/search/.

Venzke, E., 2023, Volcanoes of the World:, doi:https://doi.org/10.5479/si.GVP.VOTW5-2023.5.1.

425 Wech, A.G., 2021, Cataloging Tectonic Tremor Energy Radiation in the Cascadia Subduction Zone:
426 Journal of Geophysical Research: Solid Earth, v. 126, p. e2021JB022523,
427 doi:10.1029/2021JB022523.
428 Wech, A.G., 2016, Extending Alaska's plate boundary: Tectonic tremor generated by Yakutat
429 subduction: Geology, v. 44, p. 587–590, doi:10.1130/G37817.1.
430 Yabe, S., and Ide, S., 2014, Spatial distribution of seismic energy rate of tectonic tremors in subduction
431 zones: Journal of Geophysical Research: Solid Earth, v. 119, p. 8171–8185,
432 doi:10.1002/2014JB011383.
433